Inorg. Chem. **2007**, *46*, 9661–9671

Inorganic Chemistry
Article

Hybrid Molecular Material Exhibiting Single-Molecule Magnet Behavior and Molecular Conductivity

Hiroki Hiraga,[†] Hitoshi Miyasaka,*[†,‡] Kazuya Nakata,[†] Takashi Kajiwara,[†,‡] Shinya Takaishi,[†,‡] Yugo Oshima,[‡,§] Hiroyuki Nojiri,[‡,§] and Masahiro Yamashita*[†,‡]

Department of Chemistry, Graduate School of Science, Tohoku University, 6-3 Aramaki-Aza-Aoba, Aoba-ku, Sendai, Miyagi 980-8578, Japan, CREST, Japan Science and Technology Agency (JST), 4-1-8 Honcho, Kawaguchi, Saitama 332-0012, Japan, and Institute for Materials Research (IMR), Tohoku University, 2-1-1 Katahira, Sendai, Miyagi 980-8577, Japan

Received April 17, 2007

Two unique materials based on Mn_4 single-molecule magnet (SMM) clusters ($S_T = 9$) and integer or non-integer average valent platinum maleonitriledithiolate (mnt^{2-}) complexes, $[\{Mn^{II}_2Mn^{III}_2(hmp)_6(MeCN)_2\}\{Pt(mnt)_2\}_2][Pt(mnt)_2]_2\cdot 2MeCN$ (**1**) and $[\{Mn^{II}_2Mn^{III}_2(hmp)_6(MeCN)_2\}\{Pt(mnt)_2\}_4][Pt(mnt)_2]_2$ (**2**), were synthesized by the material diffusion method and electrochemical oxidation, respectively ($hmp^- =$ 2-hydroxymethylpyridinate). **1** and **2** are comprised of four and six $[Pt(mnt)_2]^{n-}$ units, respectively, in addition to a common $Mn^{II}_2Mn^{III}_2$ double-cuboidal unit, $[Mn^{II}_2Mn^{III}_2(hmp)_6(MeCN)_2]^{4+}$ (hereinafter $[Mn_4]^{4+}$). Among the $[Pt(mnt)_2]^{n-}$ units, two units in **1** and four units in **2** are coordinated with the $[Mn_4]^{4+}$ unit, forming a 1D chain of $\{–[Mn_4]–[Pt(mnt)_2]_2–\}$ for **1** and a discrete subunit of $\{[Pt(mnt)_2]_2–[Mn_4]–[Pt(mnt)_2]_2\}$ for **2**. The other two $[Pt(mnt)_2]^{n-}$ units, occupying void space of the packing, form a stacking column with the coordinating $[Pt(mnt)_2]^{n-}$ units, finally constructing hybrid frames of aggregates consisting of $[Mn_4]^{4+}$ units and $[Pt(mnt)_2]^{n-}$ units. Electronic conductivity measurements revealed that **1** is an insulator and **2** is a semiconductor with $\sigma = 0.22$ $S\cdot cm^{-1}$ at room temperature and an activation energy of 136 meV. Detailed magnetic measurements proved that the $[Mn_4]^{4+}$ units in **1** and **2** behave as SMMs with an $S_T = 9$ ground state at low temperatures. There is no significant interaction between $[Mn_4]^{4+}$ units and $[Pt(mnt)_2]^{n-}$ units, but interactions between localized spins of $[Pt(mnt)_2]^{n-}$ were detected even in **2** at low temperatures where the conductivity is electronically insulated. **2** is the first example of a hybridized material exhibiting SMM behavior and electronic conductivity.

Introduction

The design of multifunctional materials is one of the most challenging themes in the field of molecular materials science. One of the most attractive targets is magnetic/conducting bifunctional materials.[1] One way to design such materials is to hybridize in situ individual functioning parts, that is, magnetic and conducting frames, using a molecular self-assembly. Three representative hybrid materials have been synthesized so far: paramagnet/superconductor,[2] antiferromagnet/superconductor,[3] and ferromagnet/metal.[4] With emphasis on the third material, it is worth noting that Coronado et al. were the first to synthesize a hybrid material of coexisting ferromagnetic layers of $[Mn^{II}Cr^{III}(ox)_3]^-$ (ox = oxalate) and metallic layers of bis(ethylenedithio)tetrathiafulvalene (BEDT-TTF)[4a] or bis(ethylenedithio)tetraselenafulvalene (BEDT-TSF) molecules.[4b]

In our recent work on molecular nanosized magnets, such as single-molecule magnets (SMMs)[5] an single-chain mag-

---

* To whom correspondence should be addressed. E-mail: miyasaka@agnus.chem.tohoku.ac.jp (H.M.); yamasita@agnus.chem.tohoku.ac.jp (M.Y.).

[†] Tohoku University.

[‡] CREST-JST.

[§] IMR-Tohoku University.

(1) (a) Coronado, E.; Day, P. *Chem. Rev.* **2004**, *104*, 5419. (b) Enoki, T.; Miyazaki, A. *Chem. Rev.* **2004**, *104*, 5449. (c) Coronado, E.; Galán-Mascarós, J. R. *J. Mater. Chem.* **2005**, *15*, 66. (d) Ouahab, L. *Chem. Mater.* **1997**, *9*, 1909.

(2) Kurmoo, M.; Graham, A. W.; Day, P.; Coles, S. J.; Hursthouse, M. B.; Caulfield, J. L.; Singleton, J.; Pratt, F. L.; Hayes, W.; Ducasse, L.; Guionneau, P. *J. Am. Chem. Soc.* **1995**, *117*, 12209.

(3) Ojima, E.; Fujiwara, H.; Kato, K.; Kobayashi, H.; Tanaka, H.; Kobayashi, A.; Tokumoto, M.; Cassoux, P. *J. Am. Chem. Soc.* **1999**, *121*, 5581.

(4) (a) Coronado, E.; Galán-Mascarós, J. R.; Gómez-Garcia, C. J.; Laukhin, V. *Nature* **2000**, *408*, 447. (b) Alberola, A.; Coronado, E.; Galán-Mascarós, J. R.; Giménez-Saiz, C.; Gómez-García, C. J. *J. Am. Chem. Soc.* **2003**, *125*, 10774.

10.1021/ic700727n CCC: $37.00

nets (SCMs),[6,7] the discovery of their nanosize-specific magnetic properties has inspired us to use them as a magnetic frame for magnetic/conducting hybrid materials.[8] The SMM property is attributed to intrinsic characteristcs of the individual molecule, that is, the high-spin ground state (S_T) and the uniaxial anisotropy (large negative D and small E, considering the following Hamiltonian anisotropy term: $H = DS_{Tz}^2 + E(S_{Tx}^2 - S_{Ty}^2)$), the set of which creates a finite energy barrier (Δ) between spin-up and spin-down m_s states ($m_s = \pm S_T$) expressed as $|D|S_T^2$ for the integer S_T or $|D|(S_T^2 - {}^1/_4)$ for the half-integer S_T. Therefore, SMMs exhibit slow relaxation of the magnetization and quantum phenomena, for example, quantum tunneling of magnetization (QTM) between quantum states of $\pm m_s$, tunable by Δ or decoherent energy levels of quantum states. Meanwhile, SCMs can be assumed as a 1D case of SMM. We have been most interested in the correlation between relaxing local spins and conducting itinerant electrons in such superparamagnetic/conducting hybrid materials. From recent results of studies on SMM-based supramolecular oligomers[9] and network compounds,[10−15] it can be anticipated that inter-SMM interaction via conducting electrons, albeit small, has a mutual influence on both SMM properties and conductivity.

As our first approach to obtaining such materials, we chose a Mn^{II}_2/Mn^{III}_2 tetranuclear SMM, $[Mn^{II}_2Mn^{III}_2(hmp)_6(MeCN)_2(H_2O)_4](ClO_4)_4{\cdot}2MeCN$ ($hmp^- =$ 2-hydroxymethylpyridinate) (hereinafter, such an SMM unit is abbreviated as $[Mn_4]^{4+}$),[16] and $(NBu_4)[Pt^{III}(mnt)_2]$ ($mnt^{2-} =$ maleonitriledithiolate),[17] as starting materials. The $[Pt^{III}(mnt)_2]^{n-}$ unit has the potential to form a molecular aggregation having conducting property in assembling materials with cations.[18−21] The choice of such ionic starting materials ensured the coexistence of two distinct units, that is, an SMM unit and a conductible unit, by the mutual exchange of counterions. Then, we performed two synthetic reactions: (i) the diffusion reaction of respective starting materials, and (ii) electrochemical oxidation in a solution containing both starting materials. These reactions, as expected, yielded two novel compounds based on $[Mn_4]^{4+}$ SMM units and $[Pt(mnt)_2]^{n-}$ molecules, $[\{Mn^{II}_2Mn^{III}_2(hmp)_6(MeCN)_2\}\{Pt(mnt)_2\}_2][Pt(mnt)_2]_2{\cdot}2MeCN$ (**1**) and $[\{Mn^{II}_2Mn^{III}_2(hmp)_6(MeCN)_2\}\{Pt(mnt)_2\}_4][Pt(mnt)_2]_2$ (**2**), respectively. Whereas **1** is an SMM/insulator, **2** is an SMM/semiconductor possessing a frame composed of $[Pt(mnt)_2]^{n-}$ units possessing non-integer average valency. Although these materials are not initially intended materials of interplaying SMM character and high conductivity, at least, **2** is the first example of a hybridized material exhibiting both SMM behavior and electronic conductivity. In addition, the present synthetic strategies and the products obtained give us a foresight into the design of materials with coexisting superparamagnetic/conducting properties in the same temperature range. In this article, the syntheses, structures, and physical properties of **1** and **2** are presented.

Experimental Section

General Procedures and Materials. All of the syntheses were carried out under N_2 atmosphere. Solvents were dried with common drying agents and freshly distilled under N_2 before use. Starting materials $[Mn^{II}_2Mn^{III}_2(hmp)_6(MeCN)_2(H_2O)_4](ClO_4)_4{\cdot}2MeCN$[16] and $(NBu_4)[Pt^{III}(mnt)_2]$[17] were prepared following the reported methods.

$[\{Mn^{II}_2Mn^{III}_2(hmp)_6(MeCN)_2\}\{Pt(mnt)_2\}_2][Pt(mnt)_2]_2{\cdot}2MeCN$ (1). To an acetonitrile solution (1 mL) of $[Mn_4(hmp)_6(MeCN)_4(H_2O)_4](ClO_4)_4{\cdot}2MeCN$ (10 mg, 0.0067 mmol) was added an acetonitrile solution (1 mL) of $(NBu_4)[Pt(mnt)_2]$ (15 mg, 0.021 mmol). The mixture was stirred for a few minutes to produce a dark-green solution. This solution was pipetted into the bottom of a narrow glass tube (8ϕmm) and was layered with 2 mL of *n*-hexane. Black block-shaped crystals appeared after 1 day (4.41 mg, 22%). Calcd for $C_{76}H_{48}Mn_4N_{26}O_6Pt_4S_{16}$ (**1**): C, 31.11; H, 1.95;

---

(5) Reviews: (a) Christou, G.; Gatteschi, D.; Hendrickson, D. N.; Sessoli, R. *MRS Bull.* **2000**, *25*, 66. (b) Gatteshi, D.; Sessoli, R. *Angew. Chem., Int. Ed.* **2003**, *42*, 268−297. (c) Gatteschi, D.; Sessoli, R.; Villain, J. *Molecular Nanomagnets*; Oxford University Press: Oxford, U.K., 2006.

(6) (a) Clérac, R.; Miyasaka, H.; Yamashita, M.; Coulon, C. *J. Am. Chem. Soc.* **2002**, *124*, 12837. (b) Miyasaka, H.; Clérac, R.; Mizushima, K.; Sugiura, K.; Yamashita, M.; Wernsdorfer, W.; Coulon, C. *Inorg. Chem.* **2003**, *42*, 8203. (c) Ferbinteanu, M.; Miyasaka, H.; Wernsdorfer, W.; Nakata, K.; Sugiura, K.; Yamashita, M.; Coulon, C.; Clérac, R. *J. Am. Chem. Soc.* **2005**, *127*, 3090. (d) Miyasaka, H.; Madanbashi, T.; Sugimoto, K.; Nakazawa, Y.; Wernsdorfer, W.; Sugiura, K.; Yamashita, M.; Coulon, C.; Clérac, R. *Chem.—Eur. J.* **2006**, *12*, 7028. (e) Saitoh, A.; Miyasaka, H.; Yamashita, M.; Clérac, R. *J. Mater. Chem.* **2007**, *17*, 2002.

(7) Reviews: (a) Miyasaka, H.; Clérac, R. *Bull. Chem. Soc. Jpn.* **2005**, *78*, 1725. (b) Coulon, C.; Miyasaka, H.; Clérac, R. *Struct. Bonding* **2006**, *122*, 163.

(8) Miyasaka, H.; Yamashita, M. *Dalton Trans.* **2007**, 399.

(9) (a) Wernsdorfer, W.; Aliaga-Alcalde, N.; Hendrickson, D. N.; Christou, G. *Nature* **2002**, *416*, 406. (b) Tiron, R.; Wernsdorfer, W.; Foguet-Albiol, D.; Aliaga-Alcalde, N.; Christou, G. *Phys. Rev. Lett.* **2003**, *91*, 227203. (c) Hill, S.; Edwards, R. S.; Aliaga-Alcalde, N.; Christou, G. *Science* **2003**, *302*, 1015. (d) Park, K.; Pederson, M. R.; Richardson, S. L.; Aliaga-Alcalde, N.; Christou, G. *Phys. Rev. B* **2003**, *68*, 020405. (e) Wernsdorfer, W.; Bhaduri, S.; Tiron, R.; Hendrickson, D. N.; Christou, G. *Phys. Rev. Lett.* **2002**, *89*, 197201. (f) Edwards, R. S.; Hill, S.; Bhaduri, S.; Aliaga-Alcalde, N.; Bolin, E.; Maccagnano, S.; Christou, G.; Hendrickson, D. N. *Polyhedron* **2003**, *22*, 1911.

(10) Tiron, R.; Wernsdorfer, W.; Aliaga-Alcalde, N.; Christou, G. *Phys. Rev. B* **2003**, *68*, 140407.

(11) Boskovic, C.; Bircher, R.; Tregenna-Piggott, P. L. W.; Güdel, H. U.; Paulsen, C.; Wernsdorfer, W.; Barra, A.-L.; Khatsko, E.; Neels, A.; Stoeckli-Evans, H. *J. Am. Chem. Soc.* **2003**, *125*, 14046.

(12) Miyasaka, H.; Nakata, K.; Sugiura, K.; Yamashita, M.; Clérac, R. *Angew. Chem., Int. Ed.* **2004**, *43*, 707.

(13) Miyasaka, H.; Nakata, K.; Lecren, L.; Coulon, C.; Nakazawa, Y.; Fujisaki, T.; Sugiura, K.; Yamashita, M.; Clérac, R. *J. Am. Chem. Soc.* **2006**, *128*, 3770.

(14) Lecren, L.; Roubeau, O.; Coulon, C.; Li, Y.-G.; Le Goff, X. F.; Wernsdorfer, W.; Miyasaka, H.; Clérac, R. *J. Am. Chem. Soc.* **2005**, *127*, 17353.

(15) Lecren, L.; Wernsdorfer, W.; Li, Y.-G.; Vindigni, A.; Miyasaka, H.; Clérac, R. *J. Am. Chem. Soc.* **2007**, in press.

(16) Lecren, L.; Li, Y.-G.; Wernsdorfer, W.; Roubeau, O.; Miyasaka, H.; Clérac, R. *Inorg. Chem. Commun.* **2005**, *8*, 626.

(17) Davison, A.; Edelstein, N.; Holm, R. H.; Maki, A. H. *Inorg. Chem.* **1963**, *2*, 1227.

(18) Clemenson, P. I. *Coord. Chem. Rev.* **1990**, *106*, 171.

(19) Clemenson, P. I.; Underhill, A. E.; Hursthouse, M. B.; Short, R. L. *J. Chem. Soc. Dalton Trans.* **1989**, 61.

(20) (a) Underhill, A. E.; Ahmad, M. M. *J. Chem. Soc., Chem. Commun.* **1981**, 67. (b) Ahmad, M. M.; Underhill, A. E. *J. Chem. Soc., Dalton Trans.* **1982**, 1065. (c) Kobayashi, A.; Mori, T.; Sasaki, Y.; Kobayashi, H.; Ahmad, M. M.; Underhill, A. E. *Bull. Chem. Soc. Jpn.* **1984**, *57*, 3262. (d) Kobayashi, A.; Sasaki, Y.; Kobayashi, H.; Underhill, A. E.; Ahmad, M. M. *Chem. Lett.* **1984**, 305. (e) Ahmad, M. M.; Turner, D. J.; Underhill, A. E. *Phys. Rev. B* **1984**, *29*, 4796.

(21) The $(perylene)_2[Pt(mnt)_2]$ complex with a metallic conductibity is known, but the conductive contributor in this complex is the set of non-integer oxidized perylene entities: Henriques, R. T.; Alcácer, L.; Almeida, M.; Tomic. S. *Mol. Cryst. Liq. Cryst.* **1985**, *120*, 237.

N, 12.39. Found: C, 31.05; H, 1.65; N, 12.41. IR (KBr pellet, cm^{-1}) 2210, 1606, 1570, 1481, 1439, 1365, 1282, 1160, 1045, 825, 761, 673, 576.

[{$Mn^{II}_2Mn^{III}_2$(hmp)$_6$(MeCN)$_2$}{Pt(mnt)$_2$}$_4$][Pt(mnt)$_2$]$_2$ (2). Single crystals of **2** were synthesized by electrochemical oxidation in a nitrogen-saturated 20 mL glass vessel containing an acetonitrile solution (15 mL) of [Mn_4(hmp)$_6$(MeCN)$_4$(H_2O)$_2$](ClO_4)$_4$·2MeCN (10 mg, 0.0067 mmol) and (NBu_4)[Pt(mnt)$_2$] (20 mg, 0.028 mmol). Two platinum electrodes were equipped in the cell, and a constant current of 5 μA was applied. Black platelike crystals suitable for X-ray analysis and four-probe resistivity measurements were obtained after a few days (2.93 mg, 0.00077 mmol, 12%). Anal. Calcd for $C_{88}H_{42}Mn_4N_{32}O_6Pt_6S_{24}$ (**2**): C, 27.79; H, 1.11; N, 11.78. Found: C, 27.88; H, 1.22; N, 11.87. IR (KBr pellet, cm^{-1}): 2212, 1608, 1572, 1481, 1439, 1384, 1284, 1169, 1045, 825, 763, 671, 580.

Physical Measurements. Infrared spectra were measured on KBr disks with a Jasco FTIR 620 spectrophotometer. Magnetic susceptibility measurements were conducted with a Quantum Design SQUID magnetometer (MPMS-XL) in the temperature and dc field ranges of 1.8 to 300 K and −7 to 7 T, respectively. ac measurements were performed at various frequencies ranging from 1 to 1488 Hz with an ac field amplitude of 3 Oe. Experimental data were corrected for the sample holder and for the diamagnetic contribution calculated from Pascal constants.[22] Polycrystalline samples embedded in liquid paraffin were also measured. After correction for this additional diamagnetic contribution, no significant changes in the magnetic behavior were observed. Magnetizations on a single crystal of **1** and a field-aligned polycrystalline sample of **2** at 500 mK were measured with the Quantum Design SQUID magnetometer MPMS-XL attached to a ^{3}He refrigerator (IQUANTUM iHelium3) with application of up to ±1 T external field. Crystal-lattice orientation of the used single crystal of **1** was first determined by X-ray crystallography using a CCD diffractometer (Bruker, *SMART*), and the crystal (0.3 × 0.2 × 0.2 mm^3) was placed in a SQUID gelatin capsule with N-Apiezon. Electronic conductivity of the single crystals of **1** and **2** was first checked with the two-probe method at room temperature using a common tester. Four-probe ac resistance measurements of the single crystal of **2** were performed with current flow along the *a* axis of the crystal using a Quantum Design PPMS, and measurement temperature was scanned in the range of 5 to 300 K. Electrical contacts to the crystal were made with 15 μm platinum wire and carbon paste. High-field EPR measurements were performed with the Terahertz Electron Spin Resonance Apparatus in the Institute for Materials Research (TESRA-IMR),[23] Tohoku University. Radiation was produced with Gunn oscillators, backward traveling wave oscillators, and Calcinotron, which covered the frequency range of 35 to 400 GHz, and a pulsed magnetic field of up to 20 T was used in the study. The transmission method with Faraday configuration was employed for each sample.

Table 1. Crystallographic Data for **1** and **2**

compound	**1**	**2**
formula	$C_{76}H_{48}Mn_4N_{26}O_6Pt_4S_{16}$	$C_{88}H_{42}Mn_4N_{32}O_6Pt_6S_{24}$
fw	2934.48	3803.28
cryst syst	triclinic	triclinic
space group	$P\bar{1}$ (No. 2)	$P\bar{1}$ (No. 2)
λ (Mo Kα) (Å)	0.71070	0.71070
a (Å)	11.8935(9)	10.7098(9)
b (Å)	12.3996(10)	13.1750(11)
c (Å)	17.1234(14)	21.1269(18)
α (deg)	101.549(2)	100.777(2)
β (deg)	102.531(2)	103.169(2)
γ (deg)	96.167(2)	104.008(2)
V (Å^3)	2385.6(3)	2722.3(4)
Z	1	1
T (K)	100(2)	100(2)
μ (Mo Kα) (cm^{-1})	6.767	8.651
D_{calcd} (g·cm^{-3})	2.043	2.320
F_{000}	1402	1794
$2\theta_{max}$ (deg)	55	55
reflns meads.	24 527	27 421
reflns used	10 945 (R_{int} = 0.031)	12 422 (R_{int} = 0.060)
params	597	784
R1, wR2 [$I > 2\sigma(I)$][a]	0.0418, 0.0841	0.0363, 0.0604
R1, *wR2* [all data][b]	0.0565, 0.0808	0.0858, 0.1140
GOF on F^2	0.996	0.972
ρ_{max}/ρ_{min} (e$^-$Å^{-3})	0.393143/0.281212	0.9185/0.2765

[a] $R1 = \sum||F_o| - |F_c||/\sum|F_o|$. [b] $wR2 = [\sum w(F_o^2 - F_c^2)^2/\sum w(F_o^2)^2]^{1/2}$.

Crystallography. Single crystals with dimensions of 0.3 × 0.2 × 0.2 mm^3 for **1** and 0.2 × 0.15 × 0.01 mm^3 for **2** were mounted on a glass rod. Data collections were made on a Bruker *SMART* CCD diffractometer with graphite monochromated Mo Kα radiation (λ = 0.71070 Å). Integrated intensities were obtained with *SAINT*+, and *SADABS*[24] was used for absorption correction. The structures were solved by a direct method (*SHELXS-97*),[24] refined by full-matrix least-squares on F^2 (*SHELXL-97*)[24] based on observed reflections and variable parameters, and were converged with unweighted and weighted agreement factors of $R1 = \sum||F_o| - |F_c||/\sum|F_o|$ ($I > 2.00\sigma(I)$) and $wR2 = [\sum w(F_o^2 - F_c^2)^2/\sum w(F_o^2)^2]^{1/2}$ (all data). Non-hydrogen atoms were refined anisotropically. Hydrogen atoms were refined using the riding model. Details of the crystallographic data for **1** and **2** are listed in Table 1. These data have been deposited as CIFs at the Cambridge Data Centre as supplementary publication nos. CCDC-637152 for **1** and CCDC-637153 for **2**. Copies of the data can be obtained free of charge on application to CCDC, 12 Union Road, Cambridge CB21EZ, UK (fax: (+44) 1223−336-033; e-mail: deposit@ccdc.cam.ac.uk).

Results and Discussion

Syntheses and Characterization. **1** was synthesized by reacting [$Mn^{II}_2Mn^{III}_2$(hmp)$_6$(MeCN)$_2$(H_2O)$_4$](ClO_4)$_4$·2MeCN[16] with (NBu_4)[Pt^{III}(mnt)$_2$][17] in an approximately 1:4 mixing ratio in an acetonitrile/*n*-hexane layered solution. To obtain a pure-crystal sample, the concentration of (NBu_4)[Pt^{III}(mnt)$_2$] was kept to less than four times that of Mn_4 material (Experimental Section) because a dark-green precipitate was immediately formed when the reaction was performed by mixing an excess amount of (NBu_4)[Pt^{III}(mnt)$_2$]. From the formula of **1**, it was realized that this reaction involved a simple counterion exchange of the [Mn_4]$^{4+}$ unit from four ClO_4^- to four monoanionic [Pt^{III}(mnt)$_2$]$^-$ units ($S = {}^1/_2$). Meanwhile, **2** was obtained by electrochemical oxidation in an acetonitrile solution containing the starting materials in an approximately 1:3 ratio of Mn_4/[Pt(mnt)$_2$]$^-$. Because the basic structure and the valence of the [Mn_4]$^{4+}$ unit were unchanged in the obtained material (vide infra), the six [Pt(mnt)$_2$]$^{n-}$ units were not assigned to a simple set of integer states as [Pt^{III}(mnt)$_2$]$^-$ or [Pt^{II}(mnt)$_2$]$^{2-}$ species. To determine the oxidation state of [Pt(mnt)$_2$]$^{n-}$, the IR spectra of the

---

(22) Boudreaux, E. A.; Mulay, L. N. *Theory and Applications of Molecular Paramagnetism*; John Wiley and Sons: New York, 1976; pp 491−495.

(23) Nojiri, H.; Ajiro, Y.; Asano, T.; Boucher, J.-P. *New J. Phys.* **2006**, *8*, 218.

(24) *SHELXTL-PC Package*; Bruker AXS Inc.: Madison, U.S.A., 1998.

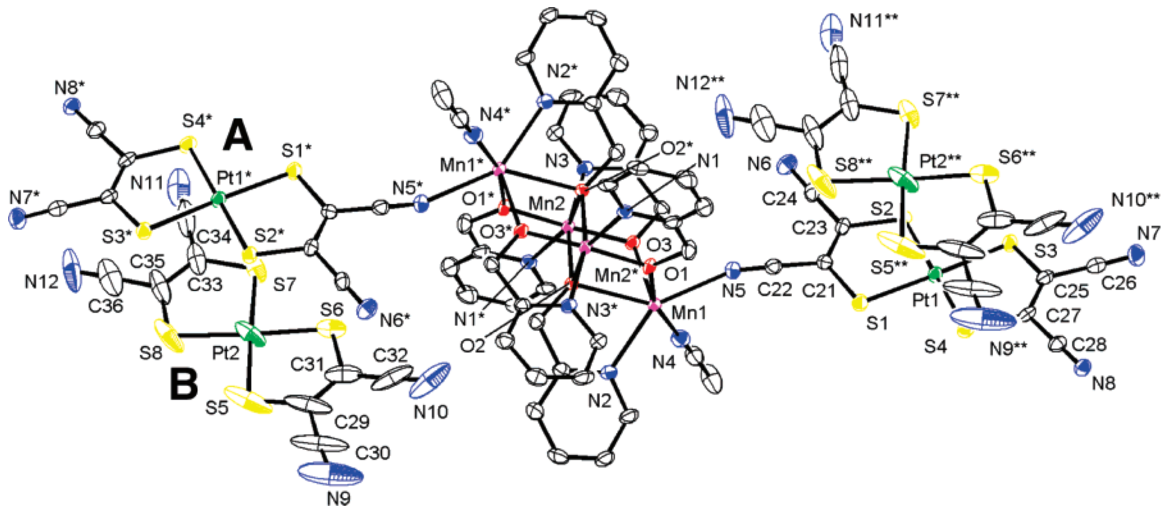

Figure 1. ORTEP view of **1** with atomic numbering scheme for selected atoms (50% probability thermal level), where symmetry operations (*): $1 - x$, $2 - y$, $1 - z$; (**): $-1 + x$, $-1 + y$, $-1 + z$.

compounds were useful; the spectra of **1** and **2** were measured on a KBr pellet in the range of 400 to 4000 $\mathrm{cm^{-1}}$. Characteristically in **2**, a charge-transfer band was found to overlap in the range of 700 to 4000 $\mathrm{cm^{-1}}$ (Figure S1 in the Supporting Information), suggesting that the degree of charge delocalization on the $[\mathrm{Pt(mnt)_2}]^{n-}$ units is larger in **2** than in **1** (study on conductivity). In addition, the sharp peak at 1365 $\mathrm{cm^{-1}}$ in **1**, which may be assignable to the $\nu_{\mathrm{C=C}}$ of the mnt^{2-} ligand,[25] appeared as a broad peak at 1384 $\mathrm{cm^{-1}}$ in **2**, although other characteristic peaks observed at frequencies higher than 1000 $\mathrm{cm^{-1}}$ were commonly found in both compounds. This indicates that the charge density distribution and the molecular symmetry on the $[\mathrm{Pt(mnt)_2}]^{n-}$ units are quite different between **1** and **2**.[26] The C≡N stretching band appeared as a sharp signal at 2210 and 2212 $\mathrm{cm^{-1}}$ for **1** and **2**, respectively, which clearly indicates the absence of $[\mathrm{Pt^{II}(mnt)_2}]^{2-}$ generally found at around 2199 $\mathrm{cm^{-1}}$.[27,28] Thus, even with such basic means of characterization as an IR measurement, we realized that **2** is probably composed of non-integer average oxidation stated (i.e., itinerant electronic stated) $[\mathrm{Pt(mnt)_2}]^{n-}$ units.[29] Indeed, these differences between **1** and **2** were responsible for the respective characteristic physical properties, particularly their conductivity (vide infra).

Structure of 1. 1 crystallized in the triclinic $P\bar{1}$ (#2) space group with $Z = 1$. An ORTEP drawing of the asymmetrical unit of **1** is depicted in Figure 1, and relevant bond distances and angles are listed in Table 2. **1** is composed of one $[\mathrm{Mn^{II}_2Mn^{III}_2(hmp)_6(MeCN)_2}]^{4+}$ double-cuboidal cluster unit and four $[\mathrm{Pt(mnt)_2}]^-$ units, where two independent $[\mathrm{Pt(mnt)_2}]^-$ units are present: coordinated ones, **A**; and uncoordinated ones, **B** (Figure 1). Despite such differences as coordinated and uncoordinated units, there are no significant differences in the intra-$[\mathrm{Pt(mnt)_2}]$ bond lengths (Table 2). The core structure of the $[\mathrm{Mn_4}]^{4+}$ unit is very similar to that of the starting $[\mathrm{Mn_4}]^{4+}$ complex,[16] where the outer manganese ions (Mn(1) and Mn(1*)) are divalent and the inner manganese ions (Mn(2) and Mn(2*)) are trivalent, as demonstrated by bond valence sum calculations. Each hexa-coordinated $\mathrm{Mn^{III}}$ ion has a distorted octahedral geometry revealing a Jahn−Teller elongation axis of [N(1*)−Mn(2)−O(2*)] with Mn(2)−O(2*) = 2.218(3) Å, Mn(2)−N(1*) = 2.206(4) Å, and N(1*)−Mn(2)−O(2*) = 160.15(15)°. In a $[\mathrm{Mn_4}]^{4+}$ unit, the Jahn−Teller axes at Mn(1) and Mn(1*) are parallel to each other. The outer $\mathrm{Mn^{II}}$ ions are hepta-coordinated with one nitrogen atom and three oxygen atoms from the chelating $\mathrm{hmp^-}$ ligands, one acetonitrile molecule, and two $[\mathrm{Pt(mnt)_2}]^-$ molecules (**A**) ($\mathrm{Mn(1)-N(8^*)_{\mathbf{A}}} = 2.384(5)$ Å and $\mathrm{Mn(1)-N(5)_{\mathbf{A}}} = 2.375(4)$ Å). The packing view is shown in Figure 2. The bonding of $[\mathrm{Mn_4}]^{4+}$ with two $[\mathrm{Pt(mnt)_2}]^-$ molecules (**A**) forms a 1D chain of $\{-[\mathrm{Mn_4}]-(\mathbf{A})_2-\}$ running along the (011) direction (part a of Figure 2). The uncoordinated $[\mathrm{Pt(mnt)_2}]^-$ units (**B**) are located between chains, forming a stairlike broken column of [**A**⋯**B**⋯**B**⋯**A**] arrangement, as shown in part b of Figure 2, in which the Pt⋯Pt distances of **A**⋯**B**, **B**⋯**B**, and intrachain **A**⋯**A** are 3.664, 3.901, and 6.907 Å, respectively. Note that the platinum ions of **A** and **B** are assigned to $\mathrm{Pt^{3+}}$ (integer state) from the charge balance, the structure, and the IR spectra, all of the $[\mathrm{Pt(mnt)_2}]^-$ units being local paramagnetic species with $S = {}^1/_2$.

Structure of 2. 2 crystallized in the triclinic $P\bar{1}$ (#2) space group with $Z = 1$. An ORTEP drawing of the asymmetrical unit of **1** is depicted in Figure 3, and relevant bond distances and angles are listed in Table 3. **2** is composed of one $[\mathrm{Mn^{II}_2Mn^{III}_2(hmp)_6(MeCN)_2}]^{4+}$ double-cuboidal unit and six $[\mathrm{Pt(mnt)_2}]^{n-}$ units, where three independent $[\mathrm{Pt(mnt)_2}]^{n-}$ units

---

(25) This assignment is not absolute, but the band is relevant to a bond frequency in $[\mathrm{Pt(mnt)_2}]^{n-}$. The corresponding band in $(\mathrm{NBu_4})_2$-$[\mathrm{Pt^{II}(mnt)_2}]$ and $(\mathrm{NBu_4})[\mathrm{Pt^{III}(mnt)_2}]$ was observed at 1383 and 1381 $\mathrm{cm^{-1}}$, respectively. For $\mathrm{K[Pt^{III}(mnt)_2]}$, see ref 26.

(26) Kutsumizu, S.; Kojima, N.; Ban, T.; Tsujikawa, I. *Bull. Chem. Soc. Jpn.* **1987**, *60*, 2547.

(27) Best, S. P.; Ciniawsky, S. A.; Clark, R. J.; McQueen, R. C. S. *J. Chem. Soc., Dalton Trans.* **1993**, 2267.

(28) The C≡N stretching band for $(\mathrm{NBu_4})_2[\mathrm{Pt^{II}(mnt)_2}]$ and $(\mathrm{NBu_4})$-$[\mathrm{Pt^{III}(mnt)_2}]$ (the starting material) was observed at 2197 and 2208 $\mathrm{cm^{-1}}$, respectively, as a strong sharp peak.

(29) The, neutral form, $[\mathrm{Pt^{IV}(mnt)_2}]$, was observed only on electrochemical oxidation: Geiger, W. E.; Barriére, F.; LeSuer, R. J.; Trupia, S. *Inorg. Chem.* **2001**, *40*, 2472.

Table 2. Relevant Bond Distances (Angstroms) and Angles (Degrees) for **1**

$[Mn_4]^{4+}$ unit	
Mn1−N2	2.263(4)
Mn1−N4	2.328(5)
Mn1−N5	2.375(4)
Mn1−N8^b	2.385(5)
Mn1−O1	2.184(3)
Mn1−O2	2.384(3)
Mn1−O3	2.162(3)
Mn2−N1^a	2.206(4)
Mn2−N3	2.039(5)
Mn2−O1^a	1.882(3)
Mn2−O2	1.956(4)
Mn2−O2^a	2.218(3)
Mn2−O3	1.873(3)
N5−Mn1−N2	147.51(18)
N5−Mn1−N4	77.27(15)
N5−Mn1−N8^b	74.10(17)
N5−Mn1−O1	88.31(14)
N5−Mn1−O2	142.28(16)
N5−Mn1−O3	82.72(15)
N1−Mn2−O2^a	160.15(15)
Coordinated $[Pt(mnt)_2]$ unit (**A**)	
Pt1−S1	2.2595(13)
Pt1−S2	2.2636(15)
Pt1−S3	2.2579(13)
Pt1−S4	2.2664(17)
S1−C21	1.708(5)
S2−C23	1.722(4)
S3−C25	1.715(5)
S4−C27	1.725(5)
C25−C27	1.364(8)
C21−C23	1.364(8)
C21−C21	1.437(7)
C23−C24	1.432(7)
C25−C26	1.446(6)
C27−C28	1.425(8)
C22−N5	1.145(6)
C24−N6	1.148(7)
C26−N7	1.144(6)
C28−N8	1.138(8)
Uncoordinated $[Pt(mnt)_2]$ unit (**B**)	
Pt2−S5	2.274(3)
Pt2−S6	2.2617(17)
Pt2−S7	2.264(2)
Pt2−S8	2.264(2)
S5−C29	1.735(10)
S6−C31	1.720(10)
S7−C33	1.712(7)
S8−C35	1.735(10)
C29−C31	1.342(11)
C33−C35	1.347(9)
C29−C30	1.446(18)
C31−C32	1.446(12)
C33−C34	1.446(14)
C35−C36	1.465(13)
C30−N9	1.147(18)
C32−N10	1.130(11)
C34−N11	1.140(14)
C36−N12	1.144(13)

[a] Symmetry operations: $1 - x, 2 - y, 1 - z$. [b] Symmetry operations: $1 - x, 1 - y, -z$.

are present: coordinated ones, **A** and **B**; and uncoordinated one, **C** (Figure 3). Similarly to **1**, variations of respective bond lengths of the $[Pt(mnt)_2]^{n-}$ units are not characteristic among **A**, **B**, and **C** units and even between **1** and **2**. The $[Mn^{II}_2Mn^{III}_2(hmp)_6(MeCN)_2]^{4+}$ unit is basically the same as that of **1**. The inner hexa-coordinated Mn^{III} ions have a Jahn−Teller elongation axis of [N(2)−Mn(2)−O(1*)] with Mn(2)−O(1*) = 2.262(6) Å, Mn(2)−N(2) = 2.207(7) Å, and N(2)−Mn(2)−O(1*) = 159.8(2)°. The outer Mn^{II} ion is hepta-coordinated with two $[Pt(mnt)_2]^{n-}$ units (**A** and **B**) with $Mn(1)-N(4)_{\mathbf{A}} = 2.409(7)$ Å and $Mn(1)-N(11)_{\mathbf{B}} = 2.321(5)$ Å, forming a discrete unit, $\{[Pt(mnt)_2]_2-[Mn_4]-[Pt(mnt)_2]_2\}$. The packing view is shown in Figure 4. The uncoordinated $[Pt(mnt)_2]^{n-}$ (**C**) and coordinated **A** and **B** are mutually stacked along the *a* axis (part a of Figure 4) to form a segregated 1D double column possessing an [**···A···B···C···**] repeat unit (part b of Figure 4), in which the Pt···Pt distances of **A···B**, **B···C**, and **C···A** are 3.577, 3.464, and 4.363 Å, respectively. Considering the charge balance, the structures of **A**, **B**, and **C**, and the IR spectra, the Pt(1), Pt(2), and Pt(3) ions have an average charge of +3.33 (non-integer average state), that is, forming $[Pt(mnt)_2]^{0.66-}$. Note that in both **1** and **2**, the easy axis of the $[Mn_4]^{4+}$ unit is aligned parallel to the same direction in their crystal packing.

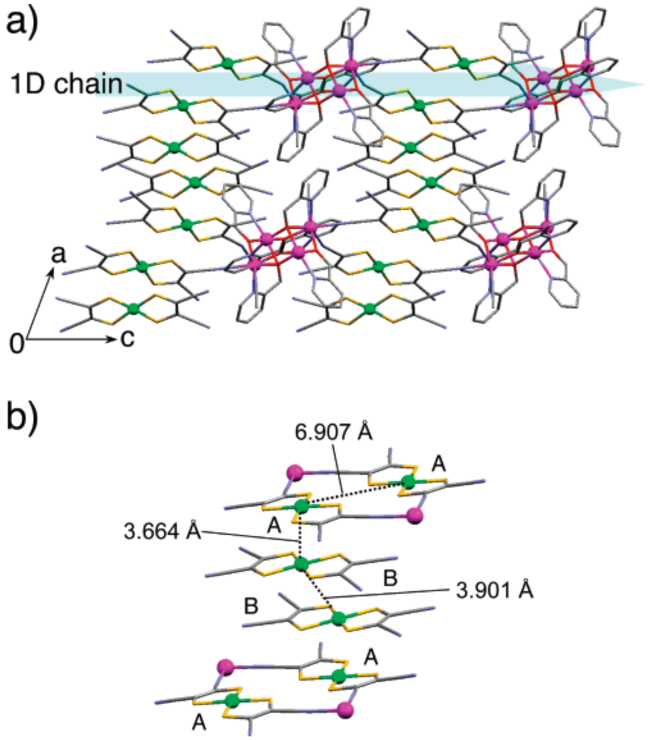

Figure 2. Packing view of **1** (a) and arrangement of part of $[Pt(mnt)_2]^{n-}$ moieties (b).

Electronic Conductivity. The electronic conductivity of the single crystals of **1** and **2** was measured by the two- and four-probe methods in the temperature range of 300 to 5 K. As expected from the IR data and the structure, **1** is an insulator ($\rho > 10^7$ Ω•cm at room temperature). In contrast, **2** shows transport property when the probes are attached in the direction of the $[Pt(mnt)_2]^{0.66-}$ column (*a*-axis direction). The conductivity at room temperature is $\sigma = 0.22$ S•cm^{-1}, which decreases gradually with decreasing temperature, and **2** is no longer conducting at approximately 110 K (Figure 5), as indicated by its semiconducting behavior with an activation energy of 136 meV, between a valence band and a conducting band. This insulating behavior with decreasing temperature would produce magnetically interacting spins on the $[Pt(mnt)_2]^{n-}$ moieties. Indeed, interactions between localized spins in the $[Pt(mnt)_2]^{n-}$ moieties were detected

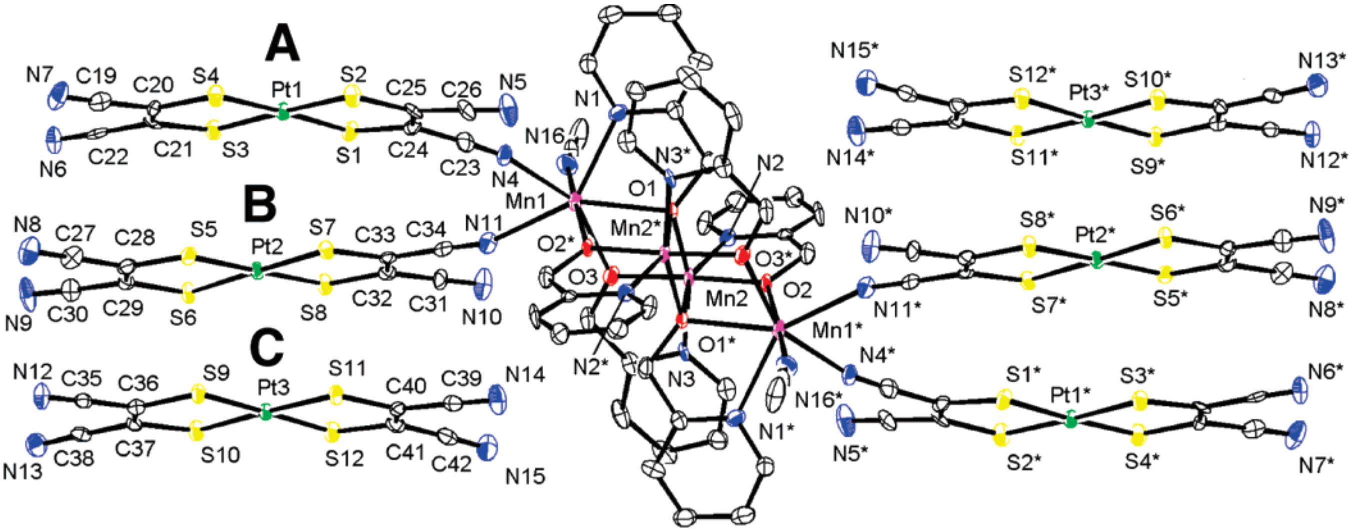

Figure 3. ORTEP view of **2** with atomic numbering scheme for selected atoms (50% probability thermal level), where symmetry operation (*): $2 - x$, $1 - y$, $2 - z$.

Table 3. Relevant Bond Distances (Angstroms) and Angles (Degrees) for **2**

	$[Mn_4]^{4+}$ unit		
Mn1−N1	2.325(6)	Mn2−O1*	2.262(6)
Mn1−N4	2.409(7)	Mn2−02	1.865(6)
Mn1−N11	2.321(5)	Mn2−O3	1.858(6)
Mn1−N16	2.250(8)	N4−Mn1−N1	79.2(2)
Mn1−O1	2.295(6)	N4−Mn1−N11	73.8(2)
Mn1−O2[a]	2.194(6)	N4−Mn1−N16	108.3(3)
Mn1−O3	2.260(5)	N4−Mn1−O1	130.23(18)
Mn2−N2	2.207(7)	N4−Mn1−O2*	79.2(2)
Mn2−N3	2.026(6)	N4−Mn1−O3	153.52(2)
Mn2−O1	1.936(5)	N3−Mn2−O1	159.8(2)
	Coordinated $[Pt(mnt)_2]$ unit (**A**)		
Pt1−S1	2.262(2)	C24−C25	1.382(11)
Pt1−S2	2.258(2)	C19−C20	1.485(13)
Pt1−S3	2.2533(19)	C21−C22	1.483(10)
Pt1−S4	2.256(2)	C23−C24	1.459(13)
S1−C24	1.716(7)	C25−C26	1.449(10)
S2−C25	1.710(9)	C19−N7	1.126(13)
S3−C21	1.727(9)	C22−N6	1.137(10)
S4−C20	1.700(7)	C23−N4	1.119(12)
C20−C21	1.339(12)	C26−N5	1.144(10)
	Coordinated $[Pt(mnt)_2]$ unit (**B**)		
Pt2−S5	2.277(2)	C32−C33	1.371(11)
Pt2−S6	2.2693(19)	C27−C28	1.459(12)
Pt2−S7	2.2700(18)	C29−C30	1.456(10)
Pt2−S8	2.272(2)	C31−C32	1.454(13)
S5−C28	1.708(7)*	C33−C36	1.468(10)
S6−C29	1.709(9)	C27−N8	1.123(12)
S7−C33	1.724(9)*	C30−N9	1.114(10)
S8−C32	1.725(7)	C34−N11	1.130(12)
C28−C29	1.409(12)	C31−N10	1.132(9)
	Uncoordinated $[Pt(mnt)_2]$ unit (**C**)		
Pt3−S9	2.262(2)	C40−C41	1.376(12)
Pt3−S11	2.2650(19)	C35−C36	1.454(13)
Pt3−S12	2.2764(19)	C37−C38	1.436(10)
Pt3−S12	2.263(2)	C39−C40	1.457(10)
S9−C36	1.712(7)	C41−C42	1.445(13)
S11−C37	1.741(9)	C35−N12	1.141(13)
S12−C40	1.734(9)	C38−N13	1.153(10)
S13−C41	1.729(7)	C39−N14	1.114(10)
C36−C37	1.354(12)	C42−N15	1.125(13)

[a] Symmetry operations: (*) 2−x, 1−y, 2−z.

by measuring high-field and high-frequency EPR (HF-EPR) spectra even in the semiconductor **2** (vide infra).

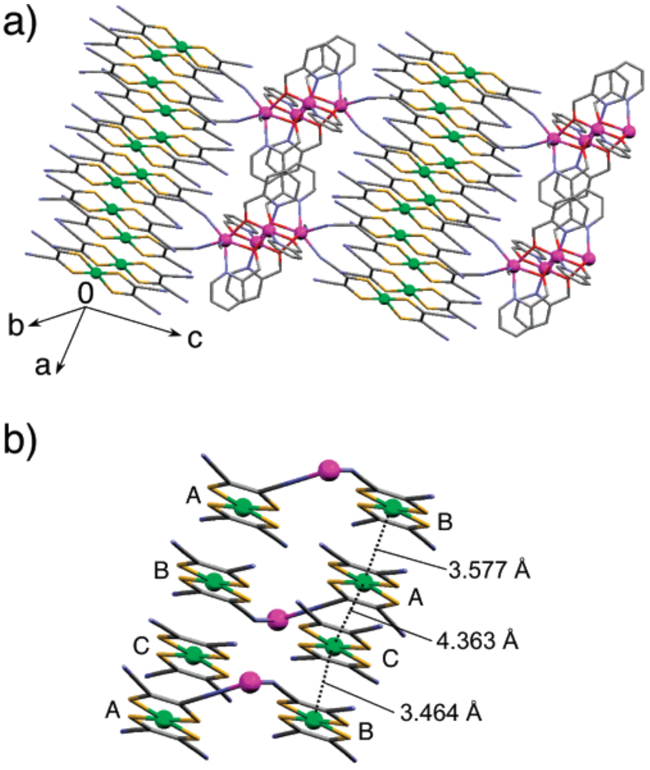

Figure 4. Packing view of **2** (a) and arrangement of part of $[Pt(mnt)_2]^{n-}$ moieties (b).

Magnetic Properties. To study the magnetic properties of these compounds, first, the temperature dependence of magnetic susceptibility was measured on a polycrystalline sample at 0.1 T in the temperature range of 1.81−300 K. Figure 6 displays χT versus T plots of **1** and **2**. The χT products of **1** and **2** increase from 17.04 and 16.44 $cm^3 \cdot K \cdot mol-1$ at 300 K to 44.10 $cm^3 \cdot K \cdot mol^{-1}$ at 2.2 K and 38.80 $cm^3 \cdot K \cdot mol^{-1}$ at 2.7 K, and then decrease slightly to 43.00 and 37.75 $cm^3 \cdot K \cdot mol^{-1}$ at 1.81 K. That the χT value of **1** at 300 K is large compared to that of only a Mn_4 cluster (15−16 $cm^3 \cdot K \cdot mol^{-1}$) is due to the contribution of four $[Pt(mnt)_2]^-$ units with $S = {}^1/_2$, whereas that of **2** is the same degree as

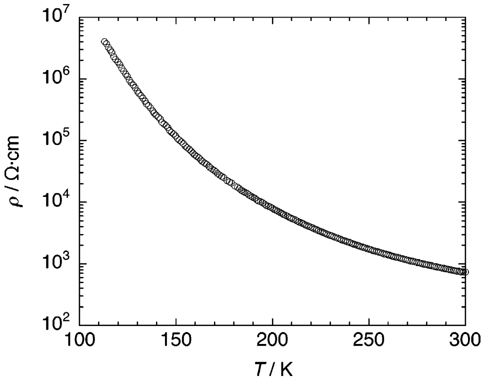

Figure 5. Temperature dependence of resistivity for a single crystal of **2** using four-probe attachment along the $[Pt(mnt)_2]^{n-}$ column.

that for an isolated $[Mn_4]$ cluster, in which the contribution from the six $[Pt(mnt)_2]^{n-}$ units should be negligible.[30] It should be noted that the entire plot displays a typical intracluster ferromagnetic behavior seen in related $[Mn_4]$ clusters.[14−16,31] The slight decrease at low temperatures is probably due to the zero-field splitting effect and/or the inter-unit antiferromagnetic interaction between $[Mn_4]^{4+}$ and $[Pt(mnt)_2]^{n-}$ units through coordination bonds, and/or between respective units through space, although the contribution of the inter-unit interaction is minimal. Therefore, to evaluate intracluster couplings between Mn^{III} ions (J_{bb}) and Mn^{III} and Mn^{II} ions (J_{wb}), the χT behavior at temperatures above 15 K was simulated based on a Heisenberg−Van Vleck model ($H_1 = -2J_{bb}(S_{Mn2}S_{Mn2*}) - 2J_{wb}(S_{Mn1} + S_{Mn1*})(S_{Mn2} + S_{Mn2*})$) that is generally employed for related compounds, where $\boldsymbol{S}_{Mn1}$ and $\boldsymbol{S}_{Mn1*}$ are the $S = {}^5/_2$ operator for Mn^{II} ions and $\boldsymbol{S}_{Mn2}$ and $\boldsymbol{S}_{Mn2*}$ are the $S = 2$ operator for Mn^{III} ions.[14−16,31] The contribution of four non-interacting $S = {}^1/_2$ spins from the $[Pt(mnt)_2]^-$ units in **1** were taken into account ($g = 2.00$). With temperature independence of paramagnetism (TIP) at 6×10^{-4} cm^3·mol^{-1} common to both compounds,[32] the following parameter sets gave respective adequate fits as shown by the red lines in Figure 6: $g = 1.99$, $J_{wb}/k_B = +0.62(2)$ K, and $J_{bb}/k_B = +4.33(6)$ K for **1**, and $g = 2.02$, $J_{wb}/k_B = +0.58(2)$ K, and $J_{bb}/k_B = +10.03(10)$ K for **2**.[33] These parameter sets are consistent with those of related $[Mn_4]$ SMM clusters[14−16,31] and induce an $S_T = 9$ ground state.

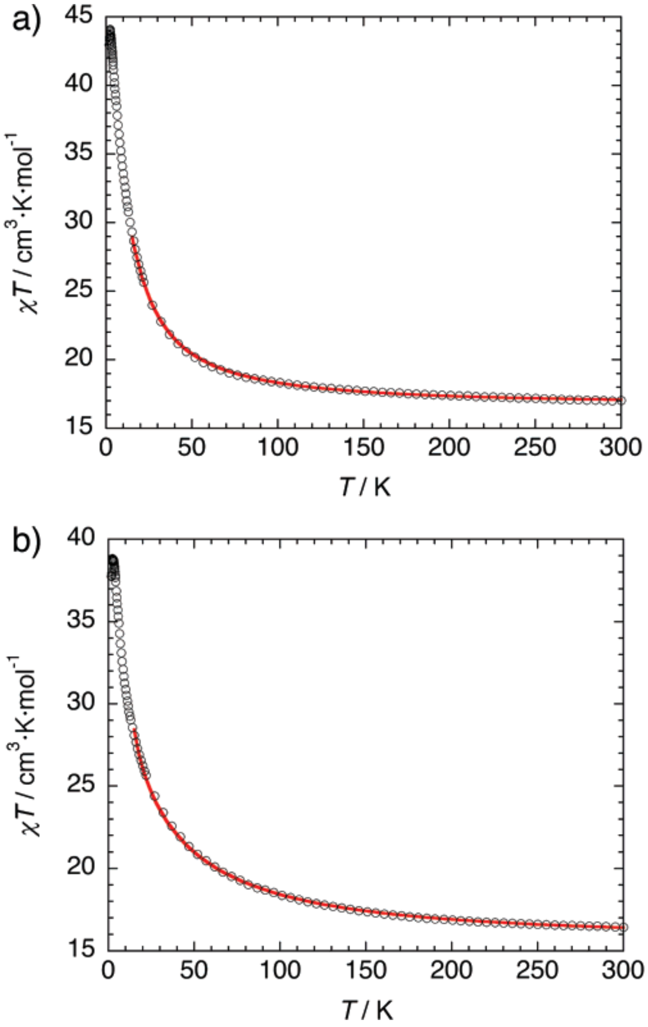

Figure 6. Temperature dependence of χT for **1** (a) and **2** (b) measured at 1 kOe. Solid lines represent the best fit obtained with a tetranuclear model, for which the contribution of four non-interacting paramagnetic species with $S = {}^1/_2$ as $g = 2.00$ is taken into account for **1** (text).

Examination of the magnetic behavior at low temperatures allows us to know the SMM character of the $[Mn_4]^{4+}$ unit and possible inter-unit interactions. The temperature dependence of ac susceptibilities measured at several ac frequencies (3 Oe ac field and zero dc field) exhibited frequency dependence of both in-phase (χ') and out-of-phase (χ'') components below 3 K (Figure 7 for **1** and Figure 8 for **2**). Within the frequency range of 1−1488 Hz, quantifiable distinct peaks of χ'' were observed only in **2** at temperatures above 1.8 K, inducing $\tau_0 = 3.8 \times 10^{-8}$ s and $\Delta_{eff}/k_B = 18.7$ K from the Arrhenius relation ($\tau(T) = \tau_0\exp(\Delta_{eff}/k_BT)$) (inset of Figure 8). Distinct peaks were detectable in both **1** and **2** as the dc field was increased and characteristic dc field dependence could be observed, as shown in Figure 9, revealing a thermal magnetization relaxation process in which

---

(30) Similar behavior neglecting the magnetic contribution of non-integer conducting columns can be seen in the following literature: Takahashi, K.; Cui, H.-B.; Okano, Y.; Kobayashi, H.; Einaga, Y.; Sato, O. *Inorg. Chem.* **2006**, *45*, 5739. Nevertheless, the treatment taking into account the contribution of four non-interacting $S = {}^1/_2$ spins from the $[Pt(mnt)_2]^-$ units was also tried for conparison (ref 33).

(31) (a) Yoo, J.; Yamaguchi, A.; Nakano, M.; Krystek, J.; Streib, W. E.; Brunel, L. C.; Hishimoto, H.; Christou, G.; Hendrickson, D. N. *Inorg. Chem.* **2001**, *40*, 4604. (b) Hendrickson, D. N.; Christou, G.; Ishimoto, H.; Yoo, J.; Brechin, E. K.; Yamaguchi, A.; Rumberger, E. M.; Aubin, S. M. J.; Sun, Z.; Aromí, G. *Polyhedron* **2001**, *20*, 1479. (c) Yang, E. C.; Harden, N.; Werndorfer, W.; Zakhrov, L.; Brechin, E. K.; Rheingold, A. L.; Christou, G.; Hendrickson, D. N. *Polyhedron* **2003**, *22*, 1857. (d) Lecren, L.; Wernsdorfer, W.; Li, Y.-G.; Roubeau, O.; Miyasaka, H.; Clérac, R. *J. Am. Chem. Soc.* **2005**, *127*, 11311.

(32) The TIP contribution has been added in the simulation for some $[Mn_4]$ clusters reported previously (refs 13−16 and 31). Furthermore, it is known that $[Pt(mnt)_2]^-$ has a large TIP at $\sim 10^{-4}$ cm^3·mol^{-1}: Uruchi, M.; Yakushi, K.; Yamashita, Y.; Qin, J. *J. Mater. Chem.* **1998**, *8*, 141. Therefore, in comparison with the data of $[Mn_4]$ clusters reported previously, the contribution of TIP at 6×10^{-4} cm^3·mol^{-1} was considered in the present simulation.

(33) If the contribution of four non-interacting $S = {}^1/_2$ spins from the $[Pt(mnt)_2]^-$ units was effective even for **2**, the χT can be also well simulated with $g = 1.92$, $J_{wb}/k_B = 0.69(1)$ K, and $J_{bb}/k_B = 10.90(10)$ K, but the obtained g value is very small.

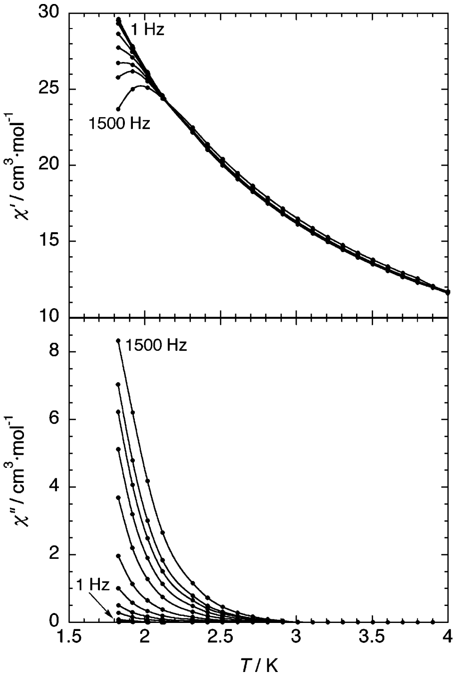

Figure 7. Temperature dependence of ac susceptibilities of **1** measured at several frequencies in the range of 1−1500 Hz.

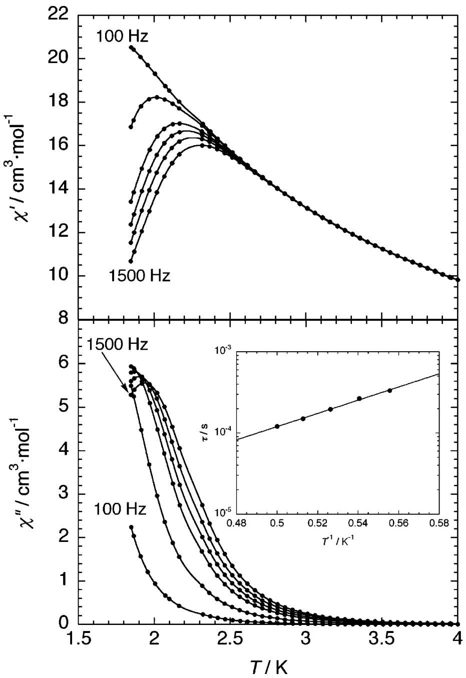

Figure 8. Temperature dependence of ac susceptibilities of **2** measured at several frequencies in the range of 100−1500 Hz.

quantum tunneling of the magnetization (QTM) is suppressed.[34] Figure 10 shows the field dependence of relaxation time estimated from the data of Figure 9. The Δ_{eff} value was changed to 20.8 K at 1700 Oe for **1** and 21.9 K at 600 Oe for **2**, where these values were obtained by measuring temperature dependence of ac susceptibility (e.g., Figure 11 for **1**). These behaviors prove that the $[\text{Mn}_4]^{4+}$ unit in **1** and **2** has SMM character. It should be noted that we could observe in **1** a growing small anomaly of χ'' in the low-frequency region in addition to the frequency-/field-dependent main signals in the high-frequency region (Figure 11). This anomaly might be due to interactions between the $[\text{Mn}_4]^{4+}$ units via the coordinating $[\text{Pt(mnt)}_2]^-$ units, although it should be very weak, but it is not certain because this effect

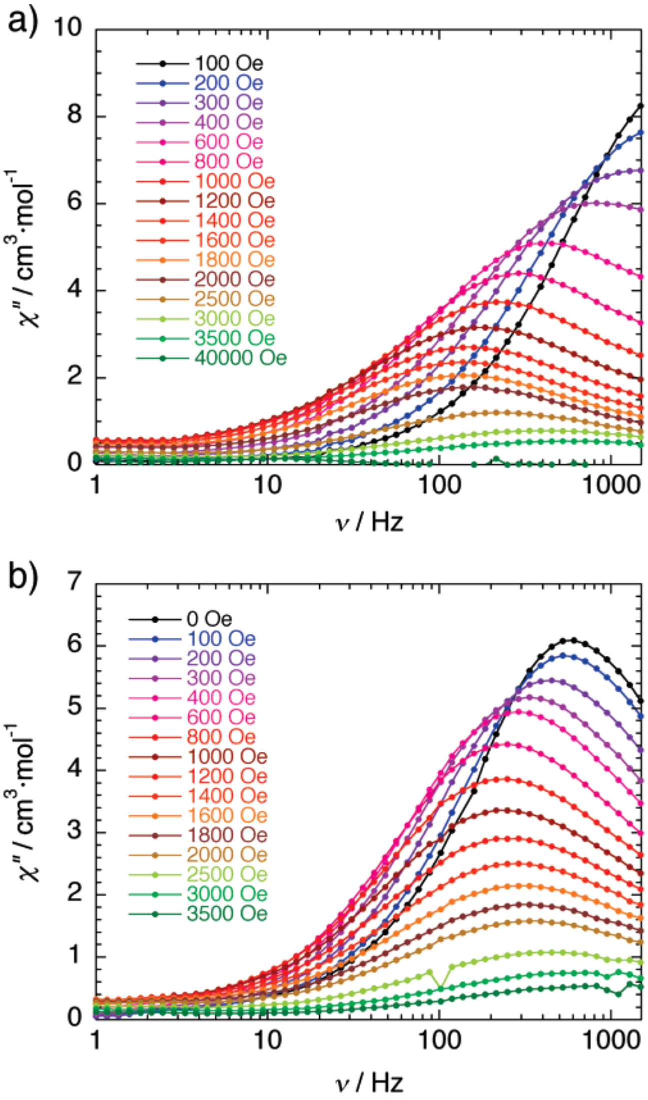

Figure 9. Frequency dependence of χ'' for **1** (a) and **2** (b) at 1.8 K as a function of the dc field.

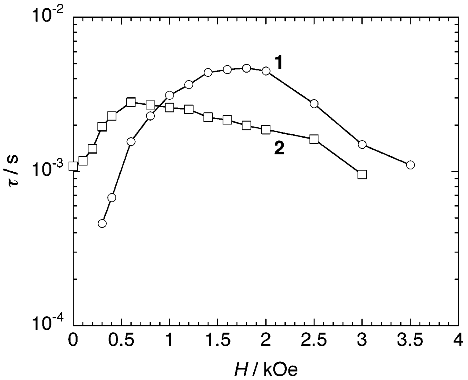

Figure 10. Field dependence of relaxation time (τ) estimated from the peak top of χ'' in Figure 9.

---

(34) (a) Ako, A. M.; Mereacre, V.; Hewitt, I. J.; Clérac, R.; Lecren, L.; Anson, C. E.; Powell, A. K. *J. Mater. Chem.* **2006**, *16*, 2579. (b) Kachi-Terajima, C.; Miyasaka, H.; Saitoh, A.; Shirakawa, N.; Yamashita, M.; Clérac, R. *Inorg. Chem.* **2007**, *46*, 5861.

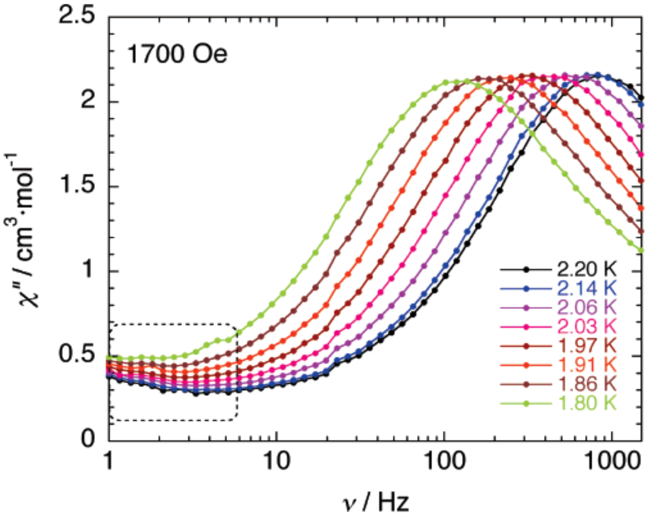

Figure 11. Frequency dependence of χ'' for **1** at 1700 Oe as a function of temperature. An anomaly could be seen in the low-frequency region (dotted square).

does not affect the essentials of the $[Mn_4]^{4+}$ SMM as confirmed by other magnetic data. To obtain further information on SMM behavior, the field dependence of the magnetization was measured on field-oriented single crystals of **1** and **2** at 470 mK with a 2 Oe/s sweep rate (Figure 12). For both compounds, a hysteresis loop typical of SMM was observed with distinct two steps (H_1 and H_2), although the coercivity of **1** was smaller than that of **2** (170 Oe for **1** and 900 Oe for **2**). The central step (H_1) of the hysteresis associated with the ground-state QTM shifted to ± 200 Oe for **1**, whereas it was observed at zero field for **2**. Neglecting ambiguity of the crystal orientation, this shift in **1** confirms the presence of weak inter-unit antiferromagnetic interaction (zJ') already suggested by the anomaly of low-frequency ac susceptibility under dc fields, where zJ' is defined in a Hamiltonian $H = H_1 + 2zJ'\langle S_T\rangle$ using a mean-field approximation with the number (z) of interacting neighbor units. Nevertheless, the estimated zJ' value is approximately -0.001 K and is negligible.[35] Thus, the $[Mn_4]$ SMM magnetism is almost isolated in the magnetic systems of **1** and **2**, even if the paramagnetic $[Pt(mnt)_2]^{n-}$ units are linked to the $[Mn_4]$ SMM unit. The second step (H_2) was observed at ca. 3000 Oe for both compounds; however, it remains uncertain if the second anomaly is due to QTM from $m_s = +9$ to $m_s = -8$.

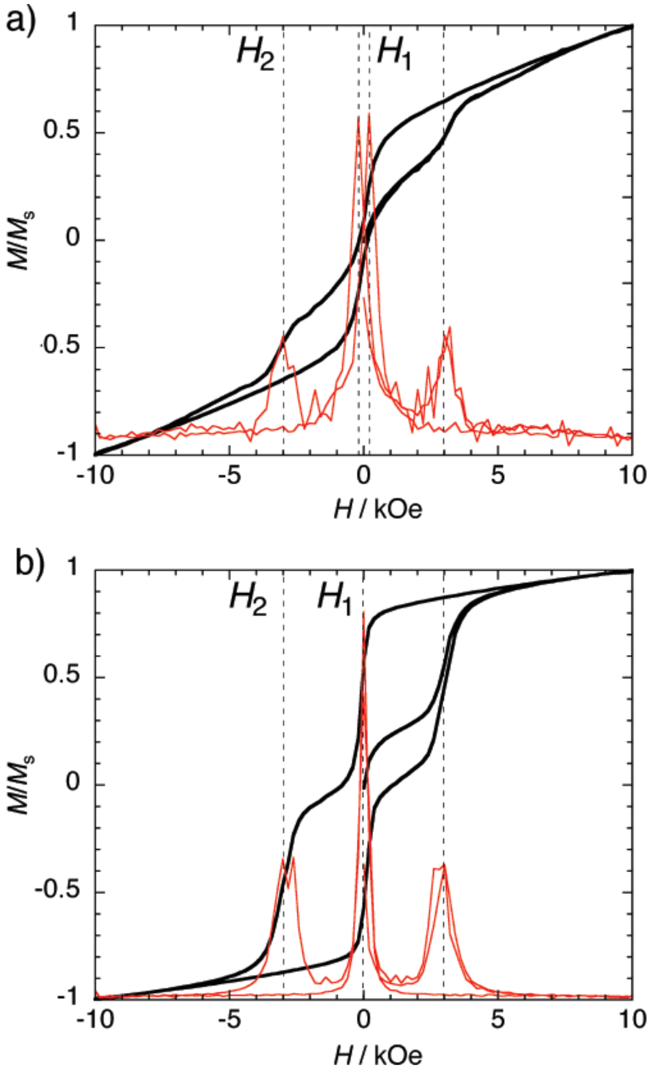

Figure 12. Field dependence of magnetization measured on field-oriented single crystals of **1** (a) and **2** (b) at 470 mK and 2 Oe/s. Red lines represent dM/dH plots (arbitrary scale).

High-Field and High-Frequency EPR. Finally, to determine the correlation between $[Mn_4]^{4+}$ and $[Pt(mnt)_2]^{n+}$ units, HF-EPR was measured on polycrystalline samples of **1** and **2**. Figure 13 shows the temperature dependence of the EPR spectra for **1** and **2** at 190 GHz. The two spectra have similar features: a strong P1 signal and a weak and broad P2 signal were observed in both, in addition to a sharp P3 signal only for **2**. The P1 signal that is assigned to the easy-axis component of the $[Mn_4]^{4+}$ ground state is independent of temperature below 40 K. Figure 14 shows field-frequency diagrams of the EPR signals of **1** and **2** at 1.6 K and the behavior of the P1 signal derived from the parameter set of $g = 1.99$ and $D_{ST}/k_B = -0.25(5)$ K for **1** and $g = 1.98$ and $D_{ST}/k_B = -0.30(5)$ K for **2** (Figure 14),[36] consistent with the values derived previously from related compounds. From the relation $\Delta = |D_{ST}|S_T^2$, we deduce $\Delta/k_B = 20.3$ and 24.3 K for **1** and **2**, respectively, which well explain the value obtained in the ac magnetic studies under dc fields. Importantly, the temperature independence of the P1 signal confirms that the inter-unit interaction by which $[Mn_4]^{4+}$ units are coordinated (superexchange interaction) is negligible: Any significant inter-$[Mn_4]^{4+}$ interaction would shift the P1 signals, as demonstrated in an SCM.[37] Another type of resonance signal, P2, appears as a conventional paramagnetic resonance with $g = 1.98$ above 20 K, as shown in Figure 13. The absence of zero-field splitting indicates clearly that the signals are caused by the localized spin of platinum (S

---

[35] The zJ' value was deduced from the H_1 field using the equation of $H_1 \approx 2z|J'|S_Tg/\mu_B$ as $S_T = 9$. See refs 9a and 9b.

[36] The g value could be estimated from the slope of P1 signal. The D value of the ground state was approximated from the following relation: $E_g = D(2S\text{-}1)$. For **1** and **2**, assuming that $S = 9$ and $D < 0$, 17D ≈ 90.1 GHz and 17D ≈ 104.8 GHz, respectively. See ref 37.

[37] Oshima, Y.; Nojiri, H.; Asakura, K.; Sakai, T.; Yamashita, M.; Miyasaka, H. *Phys. Rev. B* **2006**, *73*, 214435.

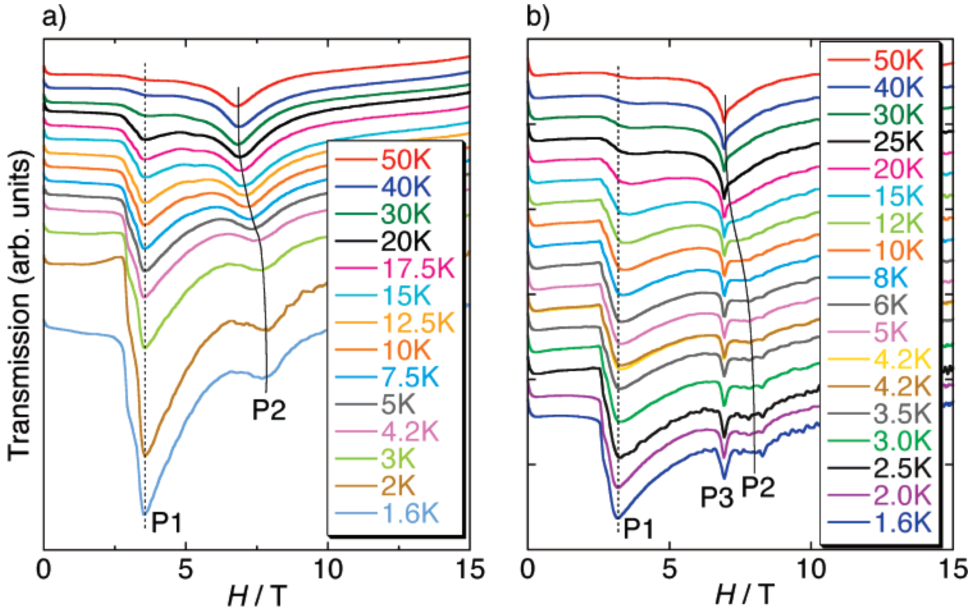

Figure 13. Temperature dependence of EPR signals measured on a polycrystalline sample of **1** (a) and **2** (b) at 190 GHz.

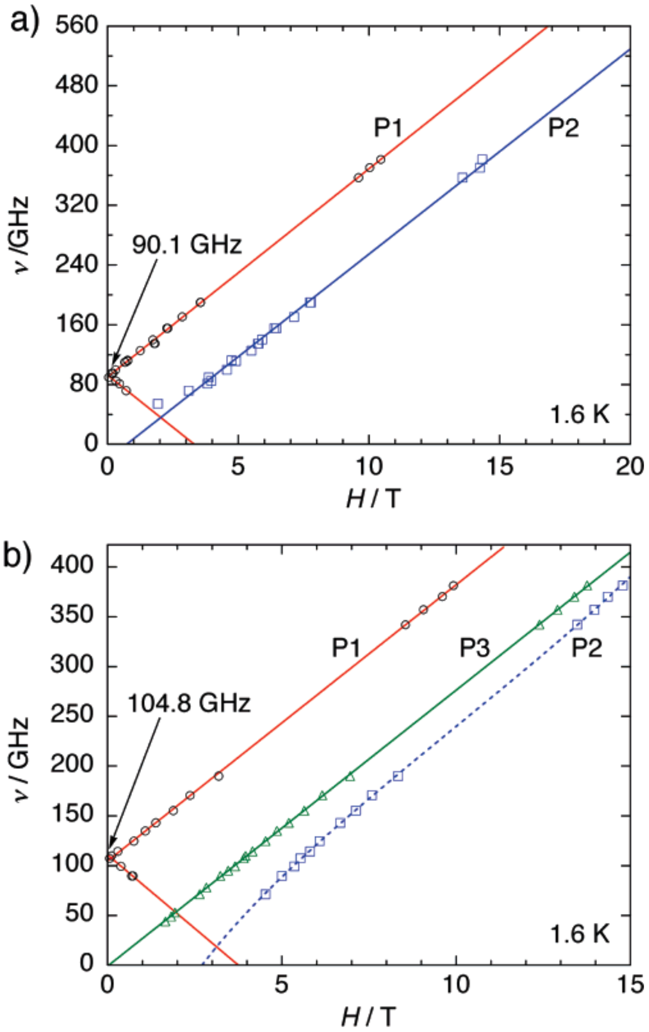

Figure 14. Field-frequency diagrams of EPR signals of **1** (a) and **2** (b) at 1.6 K. D and g values of the $[Mn_4]^{4+}$ unit were deduced from P1 plots (text).

$= {}^1/_2$). Interestingly, a considerable shift was found at low temperature, and concomitantly, the line width shows a small broadening with decreasing temperature,[38] which is the fingerprint of short-range correlation.[39] More importantly, the resonance field of the P2 signal is markedly shifted from the expected paramagnetic position at low temperatures, as shown in Figure 14, clearly demonstrating finite magnetic coupling among $[Pt(mnt)_2]^{n-}$ spins. This behavior contrasts that of the P3 signal that shows no shift even at the lowest temperature. The P3 signal is assigned to the resonance of magnetically isolated or impurity spins of $[Pt^{III}(mnt)_2]^-$. Its narrow line width, which is not expected of manganese spins, also supports this assignment. The appearance of two types of $[Pt(mnt)_2]^{n-}$ spin signals may correspond to the presence of two kinds of $[Pt(mnt)_2]^{n-}$ charge states in **2**. It is also noted that the P2 signal is less intense in **2** than in **1**. Possible reasons for this are the reduction of spin polarization or the increase in the relaxation rate. These behaviors may be caused by the semiconducting nature of **2**.

The overall features indicate that the spin state of $[Pt(mnt)_2]^{n-}$ changes with the molecular oxidation state as temperature is decreased and that there is finite coupling between $[Pt(mnt)_2]^{n-}$ spins.

Conclusions

Two unique materials **1** and **2** based on the $[Mn_4(hmp)_6(MeCN)_2]^{4+}$ SMM unit and the electron-conductible $[Pt(mnt)_2]^{n-}$ unit were selectively synthesized by two methods, the material diffusion method and electrochemical oxidation, respectively. In both compounds, the $[Mn_4(hmp)_6(MeCN)_2]^{4+}$ unit was preserved, whereas the $[Pt(mnt)_2]^{n-}$ unit was present in 1:4 and 1:6 ratios of $[Mn_4]^{4+}/[Pt(mnt)_2]^{n-}$ for **1** and **2**, respectively. **1** has an SMM/insulating character, whereas **2** exhibits an SMM/semiconducting character. It is interesting to note that such an example as **2** in which non-

---

(38) A quantitative analysis is difficult for the use of a powder specimen because we cannot separate between the change of line width and the distribution of the shift for the powder specimen.

(39) Nagata, K.; Tazuke, Y. *J. Phys. Soc. Jpn.* **1972**, *32*, 337.

integer oxidized $[Pt(mnt)_2]^{n-}$ subunits allowed conductivity is rare; only lithium salts of $[Pt(mnt)_2]^{n-}$ have been reported so far.[20] However, the conductivity was present only in the temperature region, where the SMM unit behaved as a general paramagnet. In addition, both characteristic components of SMM and conducting aggregations acted independently in the entire temperature range. Nevertheless, this work is the first to open doors to the design of superparamagnetic/*highly* conductive hybrid materials. As found in ac susceptibility, M versus H, and in HF-EPR studies of **1**, the short-range correlation of $[Pt(mnt)_2]^{n-}$ spins might be biased by $[Mn_4]^{4+}$ clusters. Such a coupling (or an effect) between the SMM part and the paramagnetic part is the first step for the crossbreeding of SMM and molecular conductors. The modification of respective starting materials and the variation of their combination would make it possible to yield intriguing materials composed of sets of SMM and conductible molecules.

Acknowledgment. This work was financially supported by the CREST project, Japan Science and Technology Agency (JST), and by a Grant-in-Aid for Scientific Research (Grant 18685007) on Priority Areas (Grant 18033042 “Chemistry of Coordination Space”) from the Ministry of Education, Culture, Sports, Science, and Technology, Japan (H.M.).

Supporting Information Available: Crystallographic data in CIF format. This material is available free of charge via the Internet at http://pubs.acs.org.

IC700727N